HHS Public Access

Author manuscript

Nat Med. Author manuscript; available in PMC 2019 March 11.

Published in final edited form as:

Nat Med. 2017 November ; 23(11): 1298–1308. doi:10.1038/nm.4412.

Activation of intestinal hypoxia-inducible factor 2α during obesity contributes to hepatic steatosis

Cen Xie[1], **Tomoki Yagai**[1], **Yuhong Luo**[1], **Xianyi Liang**[2,3], **Tao Chen**[4], **Qiong Wang**[1], **Dongxue Sun**[1], **Jie Zhao**[1], **Sadeesh K Ramakrishnan**[5], **Lulu Sun**[2,3], **Chunmei Jiang**[2,3], **Xiang Xue**[5], **Yuan Tian**[6], **Kristopher W Krausz**[1], **Andrew D Patterson**[6], **Yatrik M Shah**[5], **Yue Wu**[4], **Changtao Jiang**[2,3,7], and **Frank J Gonzalez**[1,7]

[1]Laboratory of Metabolism, Center for Cancer Research, National Cancer Institute, National Institutes of Health, Bethesda, Maryland, USA.

[2]Department of Physiology and Pathophysiology, School of Basic Medical Sciences, Peking University, Beijing, China.

[3]Key Laboratory of Molecular Cardiovascular Science, Ministry of Education, Beijing, China.

[4]Department of Internal Medicine, Key Laboratory of Environment and Genes Related to Diseases, First Affiliated Hospital of Xi'an Jiaotong University, Xi'an, Shaanxi, China.

[5]Departments of Molecular & Integrative Physiology, Division of Gastroenterology, University of Michigan Medical School, Ann Arbor, Michigan, USA.

[6]Department of Veterinary and Biomedical Sciences and the Center for Molecular Toxicology and Carcinogenesis, The Pennsylvania State University, University Park, Pennsylvania, USA.

[7]These authors jointly directed this work.

Abstract

Nonalcoholic fatty liver disease is becoming the most common chronic liver disease in Western countries, and limited therapeutic options are available. Here we uncovered a role for intestinal hypoxia-inducible factor (HIF) in hepatic steatosis. Human-intestine biopsies from individuals with or without obesity revealed that intestinal HIF-2α signaling was positively correlated with body-mass index and hepatic toxicity. The causality of this correlation was verified in mice with an intestine-specific disruption of *Hif2a*, in which high-fat-diet-induced hepatic steatosis and obesity were substantially lower as compared to control mice. PT2385, a HIF-2α-specific inhibitor, had preventive and therapeutic effects on metabolic disorders that were dependent on

Correspondence should be addressed to F.J.G. (gonzalef@mail.nih.gov), Changtao Jiang (jiangchangtao@bjmu.edu.cn), and Y.W. (yue.wu@xjtu.edu.cn).

AUTHOR CONTRIBUTIONS

C.X., T.Y., Y.L., X.L., T.C., Q.W., D.S., J.Z., S.K.R., L.S., Chunmei Jiang, X.X., Y.T., and K.W.K. performed the research and analyzed the data. C.X., A.D.P., Y.M.S., Y.W., Changtao Jiang and F.J.G. designed and supervised the research. C.X., Changtao Jiang and F.J.G. wrote the manuscript.

COMPETING FINANCIAL INTERESTS

The authors declare no competing financial interests.

Note: Any Supplementary Information and Source Data files are available in the online version of the paper.

intestine HIF-2α. Intestine HIF-2α inhibition markedly reduced intestine and serum ceramide levels. Mechanistically, intestine HIF-2α regulates ceramide metabolism mainly from the salvage pathway, by positively regulating the expression of *Neu3*, the gene encoding neuraminidase 3. These results suggest that intestinal HIF-2α could be a viable target for hepatic steatosis therapy.

Nonalcoholic fatty liver disease (NAFLD), characterized by the accumulation of ectopic triglycerides in the liver without excess alcohol consumption, is becoming te most common chronic liver disease in industrialized countries[1]. Persistent NAFLD triggers increased risk of nonalcoholic steatohepatitis (NASH) and end-stage liver diseases such as cirrhosis and hepatocellular carcinoma[2]. Obesity is a well-recognized risk factor for NAFLD. Options for pharmacologic therapy that targets NAFLD remain extremely limited[3].

Accumulating reports indicate that HIFs, members of the basic helix-hoop-helix Per-Arnt-Sim (bHLH-PAS) transcription-factor family, exert a pivotal role during the pathogenesis of NAFLD[4]. HIF is a heterodimer of an oxygen-sensitive α subunit and a constitutively expressed β subunit (HIF-1β, or ARNT)[5]. Under normoxic conditions, HIF-α (HIF-1α and HIF-2α) is rapidly hydroxylated and degraded by several prolyl hydroxylase domain enzymes (PHD), followed by conjugation with the von Hippel–Lindau (VHL) E3 ubiquitin-ligase complex. Conversely, the HIF proteins are stabilized during hypoxia, owing to the inhibition of PHD activity induced by low O_2 (refs. 6,7). Hepatocyte-specific disruption of PHD2 and PHD3 or VHL, which leads to overexpression of both HIF-1α and HIF-2α, was demonstrated to promote hepatic steatosis[8]. Hepatic HIF-2α, but not HIF-1α, was further identified as a major regulator of hepatic lipid metabolism through the upregulation of genes involved in fatty acid synthesis (*Srebf1* (also known as *Srebp1c*) and *Fasn*) and fatty acid uptake (*Cd36*) and through the downregulation of genes involved in regulating fatty acid β-oxidation (*Ppara* and *Acox1*)[9]. Most studies of the relationship between HIF and NAFLD focused on evaluating the effects of liver HIF. However, liver HIF-2α activation was recently observed to ameliorate hyperglycemia through the insulin-dependent pathway with increased insulin receptor substrate-2 (IRS2), or the insulin-independent pathway with the repression of glucagon action[10–12]. These studies imply that pharmacological inhibition of liver HIF-2α might not be suitable for NAFLD therapy, owing to the increased risk of elevating hepatic glucose production and thus aggravating type 2 diabetes. However, several novel targets in the intestine were recently implicated in the development of NAFLD[13–15]. Although both HIF-1α and HIF-2α are expressed in the intestinal epithelial cells, the role of intestinal HIF-α on the pathogenesis of NAFLD and other metabolic diseases is poorly understood.

Herein, we adopted the intestine-specific knockout or activation of HIF-α and metabolomics-profiling analysis to clarify the role and dissect the precise mechanism of intestinal HIF-α in NAFLD development. This study revealed that intestinal HIF-2α but not HIF-1α signaling is activated during obesity. Intestine-specific *Hif2a* (officially known as *Epas1*) ablation substantially ameliorates high-fat diet (HFD)-induced obesity and hepatic steatosis in mice. Improvement of the adverse metabolic phenotypes is correlated with alterations in ceramide metabolism. We identified *Neu3*, which encodes a key enzyme in the ceramide salvage pathway, as a novel target gene of HIF-2α transcriptional activity and

discovered that the HIF-2α–NEU3–ceramide axis promotes NAFLD development. Notably, we found that a specific HIF-2α inhibitor, PT2385, which is in clinical trials for the treatment of renal cancer, prevents and reverses metabolic disorders through the inhibition of intestinal HIF-2α. This work suggests that intestinal HIF-2α is a novel target for the treatment of NAFLD.

RESULTS

Intestinal HIF-2α signaling is activated in humans with obesity

To investigate the potential association between HIF-2α signaling and obesity, we assessed HIF-2α expression in distal ileum biopsies from nonobese individuals and individuals with obesity by immunohistochemical staining (Fig. 1a) and western blot analysis (Fig. 1b), revealing notably higher HIF-2α expression in humans with obesity relative to nonobese controls. The mRNA levels of *DMT1* and *DCYTB* (officially known as *CYBRD1*), two genes whose transcription is targeted by HIF-2α, were also markedly upregulated in humans with obesity (Fig. 1c). By contrast, no change was noted in HIF-1α protein expression or in the mRNA levels of its target gene *PDK1* (Fig. 1a–c). Ileum *DMT1* and *DCYTB* mRNA levels were positively correlated with body-mass index (BMI), alanine aminotransferase (ALT), and aspartate aminotransferase (AST) activities (Fig. 1d and Supplementary Fig. 1a). However, no correlation was observed for *PDK1* mRNA level with any of the parameters. The human data indicated the presence of hypoxia and the activation of HIF-2α signaling in the intestine of individuals with obesity.

To test the hypothesis that the small intestines of mice fed a HFD were hypoxic, we employed the HIF-α oxygen-dependent degradation domain (ODD)-luc mice, expressing the C-terminal portion of the ODD fused to a firefly luciferase (*luc*) gene[16]. Under normoxic conditions, the ODD is hydroxylated, which results in ubiquitination and proteasomal degradation, whereas hypoxic stress inhibits hydroxylation, leading to the accumulation of luciferase in the hypoxic tissues. As compared to the chow-diet-treated mice, there was robust activation of the luciferase signal in the small intestines from the HFD-treated group (Fig. 1e), which suggests that a HFD might trigger a hypoxia response in the small intestine. Consistent with the activation of HIF-2α signaling observed in humans with obesity, a rapid and selective induction in HIF-2α expression was demonstrated as early as 1 week following HFD treatment (Supplementary Fig. 1b). A longer, 8-week treatment resulted in an augmentation in the small intestine of HIF-2α protein levels and mRNA levels encoded by the HIF-2α target genes *Dmt1*, *Dcytb*, *Epo*, and *Fpn* as compared to chow-fed control mice (Fig. 1f).

Intestine-specific HIF-2α disruption attenuated steatosis

To understand the importance of intestinal HIF-2α in the development and progression of metabolic disorders and NAFLD, we treated control mice ($Hif2a^{fl/fl}$) and intestine-specific *Hif2a*-null ($Hif2a^{\Delta IE}$) mice with a HFD for 12 weeks. Compared to the $Hif2a^{fl/fl}$ mice, $Hif2a^{\Delta IE}$ mice exhibited less body-weight gain with HFD feeding (Supplementary Fig. 2a). A glucose-tolerance test (GTT) and insulin-tolerance test (ITT) revealed that abrogation of intestinal HIF-2α substantially improved insulin sensitivity (Supplementary Fig. 2b,c).

Furthermore, H&E and Oil Red O staining showed a reduction in hepatic lipid droplets in *Hif2a*$^{\Delta IE}$ mice (Fig. 2a). *Hif2a*$^{\Delta IE}$ mice displayed significantly lower liver weights and liver weight–to–body weight ratios relative to controls (Fig. 2b,c). Hepatic triglyceride levels, hepatic and serum cholesterol levels, and serum ALT levels reflecting hepatic lipotoxicity were markedly lower in *Hif2a*$^{\Delta IE}$ mice, with no significant difference in serum triglyceride levels as compared to the *Hif2a*$^{fl/fl}$ mice (Fig. 2d–h).

Furthermore, the mRNA expression of genes involved in fatty acid transport and anabolism (*Srebp1c*, *Cidea*, *Cd36*, *Fabp1*, *Fabp4*, *Fasn*, *Scd1*, and *Elovl6*), triglyceride synthesis (*Dgat1* and *Dgat2*), and the lipid-droplet coat (*Plin2*) were all substantially reduced in *Hif2a*$^{\Delta IE}$ mice as compared to controls (Fig. 2i). By contrast, the mRNA expression of genes involved in fatty acid β-oxidation, such as *Acox2*, *Acsl1*, and *Acaa1a*, were moderately elevated in *Hif2a*$^{\Delta IE}$ mice as compared to the control mice (Fig. 2j). Although a 12-week-period of HFD feeding did not result in obvious inflammatory cell infiltration by microscopic examination, the expression levels of inflammatory cytokines and chemokines, such as *Tnfa*, *Pai1*, *Ccl2*, and *Ccl3,* were significantly lower in *Hif2a*$^{\Delta IE}$ mice than in the controls (Fig. 2k).

Disruption of *Hif2*a was restricted to the intestines of *Hif2a*$^{\Delta IE}$ mice, as revealed by lower *Hif2a* mRNA expression in the intestine, with no changes in expression in other tissues, relative to *Hif2a*$^{fl/fl}$ mice (Supplementary Fig. 2d). Western blot analysis further showed that the disruption of intestinal HIF-2α did not affect HIF-1α or HIF-2α protein levels in the livers of the mice fed a HFD (Supplementary Fig. 2e). In addition, intestinal HIF-2α disruption did not affect body-weight gain nor hepatic steatosis of mice fed a chow diet, even though there was no evident steatosis in chow-fed mice (Supplementary Fig. 2f–n).

Intestinal HIF-2α deficiency lowers ceramide levels

To further decipher the underlying mechanism by which intestinal HIF-2α affects hepatic lipid homeostasis, we employed lipidomics to analyze the metabolites in the small intestines of the *Hif2a*$^{fl/fl}$ and *Hif2a*$^{\Delta IE}$ mice fed a HFD. Multivariate analysis distinguished different metabolic profiles between the *Hif2a*$^{\Delta IE}$ and control mice (Fig. 3a). The ions leading to the separation of the *Hif2a*$^{fl/fl}$ and *Hif2a*$^{\Delta IE}$ mice were identified as ceramides, such as C16:0 (M1, *m/z* 582.5103); C18:1 (M2, *m/z* 608.5250); C18:0 (M3, *m/z* 610.5403); C20:0 (M4, *m/z* 638.5717); C22:0 (M5, *m/z* 666.6019); and C24:1 (M6, *m/z* 692.6186) (Fig. 3b). The levels of ceramides, especially the most abundant, C16:0 ceramide, were substantially lower in the small intestines of *Hif2a*$^{\Delta IE}$ mice than in those of the controls (Fig. 3c). Similar to what was observed in the small intestine, serum ceramides were also lower in *Hif2a*$^{\Delta IE}$ mice than in *Hif2a*$^{fl/fl}$ mice (Fig. 3d and Supplementary Fig. 3a,b).

Ceramides are synthesized through three different pathways (Fig. 3e): a *de novo* pathway from palmitoyl-CoA and serine, a sphingomyelinase (SMase) pathway generated by the hydrolysis of sphingomyelin and the salvage pathway generated from the catabolism of complex sphingolipids, such as from ganglioside monosialo 3 (GM3) hydrolysis[17,18]. Consequently, sphingomyelins and glucosylceramides, the two sources for ceramide synthesis from SMase and salvage pathways, were also evaluated. There was no notable change in the relative levels of sphingomyelins in the small intestine, and only a modest reduction in serum (Fig. 3f and Supplementary Fig. 3c), whereas a marked change was

detected in the relative levels of glucosylceramides in *Hif2a*$^{\Delta IE}$ mice (Fig. 3g and Supplementary Fig. 3d).

It is well established that activation of the hepatic diacylglycerol–PKC-ε pathway triggers hepatic steatosis and insulin resistance[19]. Hepatic acylcarnitine and diacylglyceride contents and PKC-ε trans-location remained unaltered in the livers of *Hif2a*$^{\Delta IE}$ mice as compared to in those of *Hif2a*$^{fl/fl}$ mice (C.X. and Y.L., unpublished data). The changes in ceramide metabolism in response to the inhibition of intestinal HIF-2α were due neither to altered lipid absorption, as revealed by measurements of intestine and fecal lipids by both lipid-assay kits and ^{1}H-NMR, nor to morphological changes of the intestine, as examined histologically (C.X., Y.T. and A.D.P. unpublished data).

Along with diminished HIF-2α signaling in the small intestine (Supplementary Fig. 3e), many mRNAs encoded by ceramide-synthesis-related genes, including *Degs2* in the *de novo* pathway, *Smpd1*, *Smpd3*, *Smpd4*, and *Enpp7* in the SMase pathway and *Neu3*, *Glb1*, and *Gba2* in the salvage pathway, were significantly downregulated in *Hif2a*$^{\Delta IE}$ mice as compared to in *Hif2a*$^{fl/fl}$ mice (Supplementary Fig. 3f,g and Fig. 3h). The mRNAs encoded by genes involved in ceramide catabolism were at similar levels in *Hif2a*$^{\Delta IE}$ mice and in controls (Supplementary Fig. 3h).

Decreased steatosis is independent of adiposity

To further exclude a decrease in adiposity as a causal factor for the observed beneficial metabolic effects after intestinal-specific HIF-2α disruption, *Hif2a*$^{fl/fl}$ and *Hif2a*$^{\Delta IE}$ mice were treated with a HFD for a short duration of 1 week that did not lead to a notable alteration of body weight (Supplementary Fig. 4a). A GTT and an ITT revealed an improvement in glucose intolerance and insulin resistance in HFD-fed *Hif2a*$^{\Delta IE}$ mice as compared to those of *Hif2a*$^{fl/fl}$ mice (Supplementary Fig. 4b,c). The energy expenditure was substantially enhanced in *Hif2a*$^{\Delta IE}$ mice, without significant changes in cumulative food intake and ambulatory activity (Supplementary Fig. 4d–h). *Hif2a*$^{\Delta IE}$ mice exhibited lower hepatic triglyceride levels and trended toward a reduction in serum ALT levels without significant changes in liver weights and liver weight–to–body weight ratios, hepatic and serum cholesterol levels, and serum triglyceride levels, as compared to *Hif2a*$^{fl/fl}$ mice (Supplementary Fig. 4i–o). The expression of hepatic *Srebp1c*, *Cidea*, *Cd36*, *Acly*, *Acaca*, *Fasn*, *Scd1*, *Elovl6*, *Dgat1*, *Dgat2*, and *Tnfa* were lower in the *Hif2a*$^{\Delta IE}$ mice relative to the controls (Supplementary Fig. 4p–r). Accompanied by the restrained HIF-2α signaling in the small intestine, the *Neu3*, *Glb1 Smpd1*, *Smpd3*, *Enpp7*, and *Degs2* mRNAs were substantially lower in the small intestine of the *Hif2α*$^{\Delta IE}$ mice as compared to floxed control mice (Supplementary Fig. 5a–d), but were unchanged in the liver white adipose tissue (WAT) of *Hif2α*$^{\Delta IE}$ mice (C.X., unpublished data).

Lipidomics analysis confirmed that small intestinal, portal and systematic ceramides were markedly diminished in *Hif2a*$^{\Delta IE}$ mice (Supplementary Fig. 5e–g). It should be noted that the portal ceramides (which are mainly derived from the intestine) were lower to a greater degree than that of systematic ceramides (31% lower relative to 19% lower) in *Hif2a*$^{\Delta IE}$ mice as compared to the floxed controls, which suggested that serum ceramide changes resulted mainly from altered ceramide synthesis in the intestine.

To explore the mechanism by which the intestinal HIF-2α–ceramide pathway affected energy expenditure, the browning-related genes of different adipose tissues were examined. As compared to the *Hif2a*$^{fl/fl}$ mice, an induction of mRNAs encoded by uncoupling protein 1 (*Ucp1*) and other key thermogenic genes was found in subcutaneous WAT (scWAT) from *Hif2a*$^{\Delta IE}$ mice without activation of thermogenic genes in brown adipose tissue (BAT) and visceral epididymal WAT (eWAT) (Supplementary Fig. 5h–j). Western blot analysis further confirmed the upregulation of UCP1 in scWAT of *Hif2a*$^{\Delta IE}$ mice (Supplementary Fig. 5k), and immunohistochemical analysis showed an increased number of UCP1-positive beige adipocytes in the scWAT of *Hif2a*$^{\Delta IE}$ mice (Supplementary Fig. 5l).

HIF-2α modulates ceramide synthesis through targeting *Neu3*

Genetic models were used to investigate whether intestinal HIF-2α activation regulated ceramide metabolism. Mice with an intestine-specific disruption of *Vhl* (*Vhl*$^{\Delta IE}$) had robust activation of both HIF-1α and HIF-2α signaling, whereas mice lacking both VHL and HIF-1α (*Vhl/Hif1a*$^{\Delta IE}$) in the intestine induced only functional HIF-2α activation[20]. Consistently, the HIF-2α signaling was markedly activated in the small intestine of *Vhl/Hif1a*$^{\Delta IE}$ mice relative to *Vhl/Hif1a*$^{fl/fl}$, as revealed by measurements of the HIF-2α target genes *Dmt1* and *Dcytb* mRNA expression (Supplementary Fig. 6a). A similar induction of the mRNA levels of *Degs2*, *Smpd1*, *Smpd3*, *Smpd4*, *Enpp7*, *Neu3*, *Glb1*, and *Gba2* was observed in *Vhl/Hif1a*$^{\Delta IE}$ mice (Supplementary Fig. 6b–d). *Neu3* mRNA expression in the small intestine was shown to be the most robust (ten-fold) induced among the genes involved in ceramide synthesis as a result of intestine HIF-2α activation (Supplementary Fig. 6d). These alterations were completely blocked by the HIF-2α antagonist PT2385 (ref. 21).

Induction of *Neu3* was observed in both single-mutant *Vhl*$^{\Delta IE}$ and double-mutant *Vhl/Hif1a*$^{\Delta IE}$ mice, but not in *Vhl/Hif2a*$^{\Delta IE}$ mice (Supplementary Fig. 6e–j). Furthermore, the expression of *NEU3* mRNA was notably greater in the ileum biopsies of humans with obesity relative to individuals without obesity and was positively correlated with BMI, ALT, AST, *DMT1* mRNA, and *DCYTB* mRNA expression (Fig. 4a–f). An upregulation of NEU3 expression was also observed in the small intestines of HFD-treated mice as compared to chow-fed mice **(**Fig. 4g). Lactosylceramide is the product of NEU3 and a substrate for GLB1 in the salvage pathway. Consistent with the gene-expression data, the relative abundance of lactosylceramide C16:0, the predominant lactosylceramide in intestine, was also markedly lower in the small intestine of *Hif2a*$^{\Delta IE}$ mice as compared to in those of *Hif2a*$^{fl/fl}$ mice (Supplementary Fig. 6k), indicating that NEU3 activity was suppressed in *Hif2a*$^{\Delta IE}$ mice. Western blot analysis also confirmed a reduction of NEU3 expression in the small intestine by selective HIF-2α ablation (Fig. 4h).

There are two putative HIF-response elements (HRE) in the promoter of *Neu3* (Fig. 4i), which was analyzed by transient transfection using a *Neu3* promoter luciferase reporter construct. In the intestine-derived HCT116 cells, the hypoxia mimic $CoCl_2$ or co-transfection with a constitutively active HIF-2α triple mutant (TM) expression plasmid markedly induced the luciferase activity (Fig. 4j). The HIF-2α TM induction of luciferase expression was further potentiated in cells incubated with $CoCl_2$. HRE1 (ΔHRE1) or HRE2 (ΔHRE2) single-deletion constructs did not change luciferase activity, whereas the activity

in both HRE (ΔHRE) deletion constructs was markedly suppressed. These results demonstrated that HIF-2α directly regulated *Neu3* expression, and the expression was activated with either one or both HREs. Chromatin-immunoprecipitation (ChIP) assays were then performed on cross-linked soluble chromatin isolated from the small intestines of $Vhl^{fl/fl}$ or $Vhl^{\Delta IE}$ mice. Primers flanking both HREs specifically amplified the DNA sequence immunoprecipitated by the HIF-2α antibody in $Vhl^{\Delta IE}$ mice whereas no amplification was noted in controls (Fig. 4k), demonstrating that HIF-2α is able to bind the *Neu3* HREs *in vivo*. Increased HIF-2α binding to the HREs in the *Neu3* promoter from the small intestine was also found in HFD-fed mice relative to controls (T.Y., unpublished data).

Intestine-derived ceramides control hepatic steatosis

To more definitively establish the connection between intestine ceramide metabolism with hepatic steatosis, *Neu3* expression and ceramide production were investigated in HCT116 cells treated with the HIF-2α inhibitor PT2385, the NEU3 inhibitor 2,3-didehydro-*N*-acetyl-neuraminic acid (DANA)[22] and si*NEU3*. PT2385 treatment completely abolished the induction of *Neu3* under hypoxia, accompanied by decreased expression of the HIF-2α target gene *DMT1* and *DCYTB* mRNAs (Supplementary Fig. 6l). Treatment with PT2385, si*NEU3* and DANA significantly blunted hypoxia-mediated induction of ceramide levels in the intestinal cell line (Supplementary Fig. 6m and Fig. 4l,m). These results suggested that the activation of HIF-2α signaling resulted in elevated ceramide production primarily through increased *Neu3* expression *in vitro*. Furthermore, oral administration of the NEU3 inhibitors DANA and naringin[23] specifically inhibited the NEU3 activity in the small intestine, but not in the liver and WAT (Supplementary Fig. 7a–c). As a result, the small intestine and serum ceramides were substantially reduced after NEU3-inhibitor treatment as compared to vehicle (Supplementary Fig. 7d,e). DANA and naringin treatment markedly attenuated hepatic steatosis and obesity in HFD-fed mice (Supplementary Fig. 7f–p).

Moreover, ceramide administered by the injection of C16:0 ceramide to $Hif2a^{\Delta IE}$ mice fed a HFD for 6 weeks resulted in increased ceramide levels in small intestine and serum that were comparable to those in vehicle-treated HFD-fed $Hif2a^{fl/fl}$ mice (Supplementary Fig. 8a,b). The administration of ceramide substantially reversed the improvement in body weight and insulin resistance in HFD-fed $Hif2a^{\Delta IE}$ mice as compared to that of $Hif2a^{fl/fl}$ mice (Supplementary Fig. 8c–f). The intestinal-specific HIF-2α-ablation mediated reduction in hepatic lipid droplets, liver weights, ratios of liver weight to body weight, hepatic triglyceride levels, hepatic cholesterol levels, and serum ALT levels was abrogated by ceramide administration (Fig. 5a–h). Ceramide eliminated the downregulation of hepatic expression of *Srebp1c*, *Cidea*, *Cd36*, *Fabp1*, *Fabp4*, *Fasn*, *Scd1*, *Elovl6*, *Plin2*, *Tnfa*, *Pai1*, *Ccl2*, and *Ccl3* mRNAs (Fig. 5i,j).

PT2385 improves steatosis by inhibiting intestinal HIF-2α

To assess the role of intestinal HIF-2α in the PT2385-improved NAFLD, we treated HFD-fed $Hif2a^{fl/fl}$ and $Hif2a^{\Delta IE}$ mice with vehicle or PT2385. PT2385 substantially prevented HFD-induced body-weight increase and insulin resistance in $Hif2a^{fl/fl}$ mice, but not in $Hif2a^{\Delta IE}$ mice (Supplementary Fig. 9a–c). Histology analysis showed that PT2385 eliminated hepatic lipid accumulation in HFD-fed $Hif2a^{fl/fl}$ mice, but had no further

inhibition on *Hif2a*$^{\Delta IE}$ mice (Supplementary Fig. 9d). *Hif2a*$^{\Delta IE}$ mice exhibited lower liver weights, ratios of liver weight to body weight, hepatic triglycerides, hepatic and serum cholesterol content, and ALT versus *Hif2a*$^{fl/fl}$ mice, and were unresponsive to the inhibition of PT2385 treatment (Supplementary Fig. 9e–k). Further, small intestine and serum ceramide levels were markedly reduced by PT2385 in the *Hif2a*$^{fl/fl}$ mice, but not in the *Hif2a*$^{\Delta IE}$ mice (Supplementary Fig. 9l,m). Accordingly, the mRNA levels of *Degs2*, *Smpd1*, *Smpd3*, *Smpd4*, *Enpp7*, *Neu3*, *Glb1*, and *Gba2* were substantially inhibited in the HFD-fed *Hif2a*$^{fl/fl}$ mice by PT2385 treatment, but remained similar in the HFD-fed *Hif2a*$^{\Delta IE}$ mice (Supplementary Fig. 10a–d). In the liver, PT2385 downregulated the mRNA expression of *Srebp1c*, *Cidea*, *Cd36*, *Fabp4*, *Fasn*, *Scd1*, *Elovl6*, *Plin2*, *Tnfa*, *Pai1*, *Ccl2*, and *Ccl3* in the *Hif2a*$^{fl/fl}$ mice, whereas no change was found in *Hif2a*$^{\Delta IE}$ mice treated with PT2385 (Supplementary Fig. 10e,f).

To further address whether selective inhibition of intestinal HIF-2α could be a therapeutic target for HFD-induced NAFLD, and to confirm whether it is a suitable drug target, we treated HFD-fed mice with obesity and hepatic steatosis with PT2385. Oral administration of PT2385 resulted in reduced body weight and improved insulin sensitivity (Supplementary Fig. 11a–c). Liver histological analysis by H&E and Oil Red O staining indicated a reduction in hepatic lipid droplets after PT2385 treatment (Fig. 6a), which was reflected by lower liver weights, ratios of liver weight to body weight, and hepatic triglycerides relative to controls (Fig. 6b–e). Hepatic and serum cholesterol levels, and serum ALT were markedly reduced after PT2385 treatment (Fig. 6f–h).

PT2385 treatment substantially inhibited HIF-2α signaling as indicated by the decreased target gene *Dmt1* and *Dcytb* mRNAs in the small intestine (Supplementary Fig. 11d). As a result, PT2385-treated mice exhibited lower ceramide levels in both the small intestine and serum relative to vehicle-treated mice, owing to suppressed HIF-2α signaling (Fig. 6i and Supplementary Fig. 11e). Consistently, the expression of mRNAs encoded by *Degs2*, *Smpd1*, *Smpd3*, *Smpd4*, *Enpp7*, *Neu3,* and *Glb1* was substantially suppressed in PT2385-treated mice (Supplementary Fig. 11f,g and Fig. 6j). Western blot confirmed the reduction of NEU3 expression by PT2385 (Fig. 6k). Hepatic mRNA expression of the genes *Srebp1c*, *Cidea*, *Cd36*, *Fabp3*, *Fabp4*, *Fasn*, *Scd1*, *Elovl6*, *Plin2*, *Tnfa*, *Pai1*, *Ccl2*, and *Ccl3* was lower in the PT2385-treatment group than in the vehicle-treated control group (Supplementary Fig. 11h,i).

DISCUSSION

Studies with hypoxic probes indicated that there is a low pO_2 at the villi tips, and inflammation and tumors further elevate epithelial hypoxia[24]. The current study demonstrated that HFD treatment promotes HIF-2α activation; however, it does not affect HIF-1α signaling in the intestine. The precise mechanism by which a HFD activates intestinal HIF-2α signaling remains unclear. The gut-bacterial-derived short-chain fatty acids (SCFAs), notably butyrate, were reported to deplete O_2 levels and activate HIF signaling in the intestinal epithelium[25,26]. SCFAs produced by the gut microbiota might contribute to induce intestinal HIF-2α expression and activation under the condition of HFD. Other gut-microbiota-derived metabolites from tryptophan and indole metabolic

pathways activate the aryl-hydrocarbon receptor (AhR) after HFD treatment[27]. HIF-2α and AhR as heterodimeric transcription factors share the same heterodimer, partner HIF-1β. Thus, there is the potential for cross-talk between the HIF-2α and AhR signaling pathways that might influence HIF-2α signaling.

Intestinal HIF-2α depletion results in less susceptibility to HFD-induced hepatic fatty liver and obesity, accompanied by a down-regulation of intestine and serum ceramide levels. The underlying mechanism revealed that intestine HIF-2α but not HIF-1α inhibition markedly suppressed intestinal-derived ceramides by directly targeting ceramide biosynthesis by the key enzyme in the ceramide salvage pathway, NEU3. Furthermore, inhibition of intestinal HIF-2α signaling by PT2385 had both preventive and therapeutic effects on NAFLD and obesity (Fig. 6l). There is a positive correlation between HIF-2α signaling in human intestine biopsies and obesity. Considering the close link between obesity and NAFLD, these findings indicate that intestinal HIF-2α signaling is activated in obesity and NAFLD and so could be a promising therapy target in humans.

Several studies highlight the potential role for compromised epithelial barrier function and immune response in NAFLD pathogenesis[14,28,29]. HIF-1α and HIF-2α were shown to influence intestinal epithelial permeability and inflammation[30,31]. HIF-1α exerts a potent protective function at the epithelial barrier by regulating adherens-junction and tight-junction genes, including claudin 1 (*Cldn1*), mucin 3 (*Muc3*), trefoil factor 1 (*Tff1*), and 5-ectonucleotidase (*Cd73*)[32–35]. It was reported that HIF-2α has a dual role in barrier function. Acute activation of HIF-2α results in the maintenance of tight-junction assemblies and barrier integrity through the upregulation of creatine kinase[36], whereas chronic activation of HIF-2α disrupts the tight junctions through an increase of caveolin 1 (ref. 37). Several reports showed that mice with intestinal epithelial HIF-1α ablation are more susceptible to intestinal injury and inflammation, whereas HIF-1α activation leads to an anti-inflammatory response in inflammatory bowel disease[38]. Prolonged HIF-2α activation in intestinal epithelial cells triggers a spontaneous inflammatory response, whereas intestinal HIF-2α deficiency substantially reduces inflammation through the direct regulation of inflammatory mediators, including tumor necrosis factor-α, microsomal prostaglandin synthase 1, and cyclooxygenase 2 in colitis models[20,39]. It cannot be excluded that improvement of the intestinal epithelial permeability and inflammation might contribute to the metabolic benefits of intestinal HIF-2α inhibition in the mouse model of obesity.

It is well established that there is a positive relationship between ceramide levels and metabolic diseases in humans and mice[40,41]. In patients with NAFLD, the serum ceramide levels are markedly increased[42,43]. A causal role of ceramides in NAFLD development was further demonstrated by using pharmacological or genetic inhibition of enzymes involved in ceramide metabolism[44]. Overexpression of acid ceramidase in either the liver or adipose tissue protects against HFD-induced hepatic lipid accumulation and insulin resistance by reducing ceramide synthesis in adipose tissue[45]. The elevated C16:0-ceramide levels induced by overexpressing ceramide synthase enzymes 6 (*Cers6*) leads to hepatic steatohepatitis and insulin resistance, whereas liver- or adipose-specific *Cers6* disruption improves fatty liver and obesity by boosting fatty acid β-oxidation[46,47]. Mice lacking dihydroceramide desaturase 1 (DEGS1) are also resistant to HFD-induced obesity and

insulin resistance, owing to lower levels of ceramides[48]. Ceramides substantially upregulate fatty acid uptake and synthesis through direct or indirect modulation of CD36 and SREBP1C signaling, respectively[15,46]. The lower levels of intestinal ceramide production led to less hepatic lipid accumulation in a gutmicrobiota-remodeling mouse model[15]. Beside the effects of ceramide on NAFLD, ceramide was also shown to impair beige-fat function, thereby lowering energy expenditure[49,50]. It is also well established that enhanced energy expenditure can improve hepatic steatosis and insulin resistance in rodent models of NAFLD[51,52]. Mice with adipocyte-specific disruption of *Sptlc2* involved in the *de novo* ceramide-synthesis pathway displayed improved beige-fat thermogenesis and hepatic steatosis following the inhibition of adipocyte ceramide synthesis[52]. Supporting this view, the current study showed that mice lacking intestine HIF-2α are resistant to HFD-induced hepatic steatosis and obesity, which is correlated with lower intestine and serum ceramides, with suppressed fatty acid synthesis and uptake, and with higher 'beiging' and thermogenic capacity. However, expression of the fatty acid β-oxidation-related genes are not changed in the livers of $Hif2a^{fl/fl}$ and $Hif2a^{\Delta IE}$ mice fed a HFD for 1 week, whereas most genes encoding fatty acid–synthesis-related enzymes are substantially downregulated in the livers of $Hif2a^{\Delta IE}$ mice, which suggests that the HIF-2α–ceramide axis mainly regulates hepatic fatty acid synthesis.

Furthermore, intestine HIF-2α but not HIF-1α was defined as a novel regulator of the ceramide salvage pathway, as revealed by measuring *Neu3*, *Glb1*, and *Gba2* mRNA expression. Notably, NEU3 catalyzes the hydrolysis of GM3 into lactosylceramides, which can be converted into glucosylceramides by GLB1, whereas GBA2 catalyzes the generation of ceramides from glucosylceramides[53]. This study revealed that *Neu3* is a direct target gene of HIF-2α. Interestingly, NEU3 overexpression in liver was observed to increase hepatic lipid accumulation and liver weight[54]. In the current study, direct inhibition of intestinal NEU3 substantially ameliorated hepatic steatosis. It was demonstrated that the ceramides themselves represent a more central modulator of obesity and hepatic steatosis than glucosylceramides, lactosylceramides, or sphingomyelins[49]. Therefore, the decrease of intestine-derived ceramide levels might contribute to the improvement of NAFLD after the inhibition of intestinal HIF-2α. Besides, NEU3 was found to be an upstream activator of HIF-1α in muscle cells[55]. Although HFD treatment elevated NEU3 expression, increased expression of HIF-1α protein was not found. The cell types and differential expression of the *Hif1a* genes may be crucial for the regulation of HIF-1α.

HIF-2α, a bHLH–PAS domain protein, was considered undrug-gable until the discovery of a class of compounds, including PT2385 (ref. 21). PT2385 is an orally bioavailable HIF-2α antagonist that specially inhibits HIF-2α transcriptional activity by allosterically blocking the heterodimerization between HIF-2α and HIF-1β, while having no effect on HIF-1α. Recent reports revealed that PT2385 and the closely related analog PT2399 inhibits tumor growth and displays better efficacy than sunitinib, a currently approved first-line anti-angiogenesis drug[21,56,57]. PT2385 is well tolerated without toxicities in a phase 1 clinical trial to treat renal cell carcinoma. In the present study, the inhibition of intestinal HIF-2α signaling by PT2385 substantially prevents and reverses obesity and hepatic steatosis, followed by a reduction of intestine and serum ceramide levels. Thus, this study revealed an

essential role for intestinal HIF-2α in regulating obesity, insulin resistance and hepatic lipid metabolism, and provided a potential therapeutic approach for treating metabolic disorders.

METHODS

Methods, including statements of data availability and any associated accession codes and references, are available in the online version of the paper.

ONLINE METHODS

Human cohorts.

Distal ileum mucosa biopsies were taken from two cohorts (n = 12 and 35, respectively). These individuals were undergoing routine colonoscopy without diagnosis for NAFLD or type 2 diabetes. The genders and ages were at similar levels at baseline in both the nonobese cohort and the cohort with obesity (Supplementary Table 1). The clinical biochemistry variables are listed in Supplementary Table 2. All indivduals fulfilled the following inclusion criteria: (i) no significant acute or chronic viral hepatitis; (ii) no significant alcohol consumption (the definition of 'significant' alcohol consumption has been inconsistent, and ranged from >1 alcoholic beverage at 10 g of alcohol per one drink unit per day to > 40 g per day); (iii) no thyroid dysfunction; (iv) no inflammatory bowel disease; (v) no pregnancy; and (vi) do not have a condition that is unsuitable for biopsy as judged by the clinician. The study was approved by Conjoint Health Research Ethics Board of the First Affiliated Hospital of Xi'an Jiaotong University, China, and written informed consent was given to all individuals before participation in this study. The biopsies from cohort 1 (n = 12) were used for immunohistochemical staining and western blot analysis. The biopsies from cohort 2 (n = 35) were used for real-time PCR analysis.

Mouse studies.

Hif2a$^{fl/fl}$, *Vhl*$^{fl/fl}$, *Vhl/Hif1a*$^{fl/fl}$, and *Vhl/Hif2a*$^{fl/fl}$ mice were previously described[58,59]. For intestine-specific disruption, *Hif2a*$^{fl/fl}$, *Vhl*$^{fl/fl}$, *Vhl/Hif1a*$^{fl/fl}$, and *Vhl/Hif2a*$^{fl/fl}$ were crossed with mice harboring the Cre recombinase under control of the villin promoter to obtain the *Hif2a*$^{\Delta IE}$, *Vhl*$^{\Delta IE}$, *Vhl/Hif1a*$^{\Delta IE}$, and *Vhl/Hif2a*$^{\Delta IE}$ mice. The *Vhl*$^{fl/fl}$, *Vhl*$^{\Delta IE}$, *Vhl/Hif1a*$^{fl/fl}$, *Vhl/Hif1a*$^{\Delta IE}$, *Vhl/Hif2a*$^{fl/fl}$, and *Vhl/Hif2a*$^{\Delta IE}$ were on a mixed Sv129 and C57BL/6 background. The *Hif2a*$^{fl/fl}$ and *Hif2a*$^{\Delta IE}$ were on a C57BL/6N background, after backcrossing with C57BL/6N mice for more than five generations. HFD (60% kcal from fat) was purchased from Bioserv (Flemington, NJ). 8- to 10-week-old male littermate *Hif2a*$^{fl/fl}$ and *Hif2a*$^{\Delta IE}$ mice were fed a chow or HFD for 12 weeks or 1 week to induce hepatic steatosis. For the ceramide turnover study, C16:0 ceramide, purchased from Avanti Polar Lipids (Alabaster, AL), was suspended in saline with 0.5% sodium carboxymethyl cellulose. 8- to 10-week-old male littermate *Hif2a*$^{fl/fl}$ and *Hif2a*$^{\Delta IE}$ mice fed a HFD and injected the intraperitoneally every other day with vehicle or C16:0 ceramide (15 mg/kg) for 6 weeks. For the NEU3-inhibitor study, DANA and naringin were purchased from Sigma-Aldrich (St. Louis, MO). DANA was dissolved in saline and naringin was suspended in saline with 0.5% sodium carboxymethyl cellulose and 5% dimethyl sulfoxide. C57B6/N mice fed a HFD with vehicle were gavaged with DANA (20 mg/kg o.p.d.) or naringin (200 mg/kg o.p.d.) for 4

weeks. For the HIF-2α inhibitor studies, PT2385, purchased from MedChem Express (Monmouth Junction, NJ), was suspended in saline with 0.5% sodium carboxymethyl cellulose, 2.5% Tween 80 and 2.5% dimethyl sulfoxide. For the treatment of hepatic steatosis, C57BL/6N mice with obesity fed a HFD for 8 weeks were administered vehicle or PT2385 (20 mg/kg o.p.d.) by gavage for another 4 weeks. To determine whether the action of PT2385 was HIF-2α dependent, 8- to 10-week-old male littermate *Hif2a*$^{fl/fl}$ and *Hif2a*$^{\Delta IE}$ mice fed a HFD were administered vehicle or PT2385 (20 mg/kg o.p.d.) by gavage for 12 weeks. For the short-term treatment, 8- to 10-week-old male littermate *Vhl/Hif1a*$^{fl/fl}$ and *Vhl/Hif1a*$^{\Delta IE}$ mice fed a chow diet were administered vehicle or PT2385 (20 mg/kg o.p.d.) by gavage for 3 d. All mice were randomly assigned to experimental groups (at least four mice per group), and the groups did not present differences in body weights before the treatments. All mouse studies were approved by the NCI Animal Care and Use Committee and performed in accordance with the Institute of Laboratory Animal Resources guidelines. All mice were fed *ad libitum* and kept in a 12-h light–dark cycle.

ODD-luciferase transgenic mice study.

ODD-luciferase transgenic mice were obtained from Jackson Laboratories (Bar Harbor, ME). 10-week-old male littermate mice were fed a chow or HFD for 1 week. Small intestines were collected and extracted with lysis buffer, and the luciferase activities were measured by use of the luciferase assay system (Promega).

Western blot analysis.

Intestine and scWAT samples were lysed in RIPA buffer with protease and phosphatase inhibitors, and then the protein extracts were separated by SDS–PAGE electrophoresis and transferred to a PVDF membrane. The membrane was incubated overnight at 4 °C with antibodies against HIF-2α (Novus Biologicals, LLC, Littleton, CO, Cat# NB100–122), HIF1α (Novus Biologicals, Cat# NB100–105), NEU3 (Origene Technologies, Rockville, MD, Cat# TA590228), β-ACTIN (Cell Signaling, Danvers, MA, Cat# 4970), UCP1 (Abcam, Cambridge, MA, Cat# ab10983), and eIF5 (Cell Signaling, Cat# 13894). The full western blot gel panels are shown in Supplementary Figure 12.

Metabolic assays.

For the glucose tolerance test (GTT), the mice were fasted overnight for 16 h. For the insulin tolerance test (ITT), the mice were fasted for 4 h. Glucose at 2 g/kg or insulin (Eli Lilly, Washington, DC) at 0.8 U/kg in saline were injected intraperitoneally to conscious animals and from tail vein, blood glucose was measured before and at 15, 30, 60, and 90 min post injection using a glucometer (Bayer, Pittsburgh, PA).

Histological analysis.

Formalin-fixed paraffin-embedded liver sections were stained by H&E and OCT-embedded frozen liver sections were stained by Oil O Red according to standard protocols followed by microscopic examination. Three discontinuous liver sections were evaluated for each mouse.

Clinical chemistry measurements.

Liver injury was evaluated by measuring alanine aminotransferase (ALT) in serum (Catachem In., Oxford, CT). Hepatic and serum triglycerides were determined with a triglyceride colorimetric assay kit (Bioassay Systems, Hayward, CA). Hepatic and serum cholesterol contents were measured using assay kit from Wako Diagnostics (Wako Chemicals USA, Richmond, VA).

Real-time PCR analysis.

The intestine mucosa was gently scraped and liver flash frozen in liquid nitrogen, and both were stored at −80 °C. Total RNA from frozen intestine mucosa and liver was extracted with TRIzol reagent (Invitrogen, Carlsbad, CA). cDNA was synthesized from 1 μg total RNA using qScript cDNA SuperMix (Gaithersburg, MD). Real-time PCR primer sequences are included in the Supplementary Table 3. The relative amount of each mRNA was calculated after normalizing to their corresponding β-actin or *Gapdh* mRNA, and the results expressed as fold change relative to the control group.

Metabolomics analysis.

Global lipidomics was performed as previously described[15]. For global lipidomics, the multivariate data matrix was analyzed by SIMCA-P+14 software (Umetrics, Kinnelon, NJ). For ceramide quantitation, the data were analyzed by TargetLynx software, a subroutine of the MassLynx software (Waters Corp.). The ceramide standards, including C16:0, C18:0, C18:1, C20:0, C22:0, C24:0 and C24:1, were obtained from Avanti Polar Lipids (Alabaster, AL).

Indirect calorimetry.

Indirect calorimetry was carried out on *Hif2a*$^{fl/fl}$ and *Hif2a*$^{\Delta IE}$ mice fed a HFD for 1 week using a 12-chamber Environment Controlled CLAMS (Columbus Instruments, Columbus, OH). After a 48-h acclimatization period, mice were monitored for 24 h at 22 °C. During testing, food and water were provided *ad libitum*.

Luciferase-reporter gene assays.

The *Neu3* promoter region was predicted by FANTOM5 mouse promoterome. Hypoxia response elements (HREs) in the promoter region were further identified by HIF-2α ChIP assay (see below). The *Neu3* promoter and the HRE-lacking promoter fragments were amplified by PCR from mouse genomic DNA. The primer sequences are listed in Supplementary Table 3. The amplified fragments were digested by KpnI and XhoI restriction enzymes (New England BioLabs), and then cloned into the pGL4.11 luciferase vector (Promega). *Neu3* reporter vectors and phRL-TK Renilla luciferase control vector (Promega) were co-transfected into HCT116 cells (ATCC CCL-247) by use of Lipofectamine 3000 transfection reagent (Thermo Fisher Scientific). In addition, either constitutively active HIF-2α triple mutants (HIF-2α−TM) expression vector[60] or the empty backbone vector (pcDNA3) were co-transfected into the cells and cobalt (II) chloride hexahydrate (Sigma-Aldrich) was added to culture medium at a 100-μM final concentration to mimic hypoxia. Empty vector (pGL4.11) was used as a negative control and the standard.

After 24 h from the transfection, luciferase assays were performed by use of the dual-luciferase assay system (Promega). Firefly and Renilla luciferase activities were measured by Veritas microplate luminometer (Turner Biosystems).

Cell treatment.

HCT116 cells were seeded in 12-well plates (for gene expression analysis) or six-well plates (for lipidomics analysis). Cells were treated with vehicle, PT2385 (10 μM), or DANA (100 μM), or transfected with si*NEU3* (20 nM, Thermo Fisher Scientific, Waltham, MA) and exposed to either vehicle or $CoCl_2$ (100 μM) for 24 h.

ChIP assay.

ChIP assays were performed as described previously, on duodenal epithelium scrapings using 1% formaldehyde in 1× PBS as a cross-linker[39]. The primary antibody for HIF-2α (Novus Biologicals) was used for immunoprecipitation. The precipitated DNA samples were incubated with RNase A and proteinase K, purified using PCR clean-up column (Qiagen), and 2 μl of sample was used for real-time PCR using primers listed in Supplementary Table 3.

Neuraminidase-activity assays.

Intestine neuraminidase activity was determined in the intestine homogenates using a Neuraminidase Activity Assay kit (Sigma-Aldrich).

Data analysis.

Statistical analysis was performed using Prism version 7.0 (GraphPad Software, San Diego, CA). To predetermine sample sizes, power analysis was performed using StatMate version 2.0 (GraphPad Software). Experimental values are presented as mean ± s.e.m. The investigators involved in this study were not completely blinded during sample collection or data analysis in animal experiments, but were blinded in human study. No animal or sample was excluded from the analysis. The sample distribution was determined by a Kolmogorov–Smirnov normality test. Correlations were assessed by nonparametric Spearman's test. Statistical significance between two groups was determined using two-tailed Student's *t*-test. One-way ANOVA followed by Tukey's *post hoc* correction was applied for multi-group comparisons. *P* values of less than 0.05 were considered to be significant.

Data availability.

The data that support the findings of this study are available from the corresponding authors upon reasonable request. Additional detailed information on experimental design and reagents for this study is provided in the **Life Sciences Reporting Summary**.

Supplementary Material

Refer to Web version on PubMed Central for supplementary material.

ACKNOWLEDGMENTS

We thank L.G. Byrd, Y. Zhang, X. Gao, W. Liu, X. Gong, and T. Yan (National Cancer Institute) for assistance with the mouse studies, and B. Liu and X. Wu (Chinese Academy of Sciences) for help with the immunohistochemistry. This project was funded in part by the National Cancer Institute Intramural Research Program to F.J.G., grants from the National Key Research and Development Program of China (2016YFC0903100, 2016YFC0903102) to Changtao Jiang, the National Natural Science Foundation of China (31401011 and 81522007 to CT. J., and 81403007 to X.C.), National Institutes of Health grants ES022186 to A.D.P., and CA148828 and DK095201 to Y.M.S. S.K.R. was supported by NIDDK (K99DK110537). Q.W. was supported by the Peak Talent Foundation of Jiangsu Province Hospital of Chinese Medicine (Y2014RC18) and Jiangsu Government Scholarship for Overseas Studies. D.S. and J.Z. were supported by fellowships from the Chinese Scholarship Council.

References

1. Ray K NAFLD-the next global epidemic. Nat. Rev. Gastroenterol. Hepatol 10, 621(2013). [PubMed: 24185985]
2. Chalasani N et al. The diagnosis and management of non-alcoholic fatty liver disease: practice guideline by the American Gastroenterological Association, American Association for the Study of Liver Diseases, and American College of Gastroenterology. Gastroenterology 142, 1592–1609 (2012). [PubMed: 22656328]
3. Rotman Y & Sanyal AJ Current and upcoming pharmacotherapy for non-alcoholic fatty liver disease. Gut 66, 180–190 (2017). [PubMed: 27646933]
4. Ju C, Colgan SP & Eltzschig HK Hypoxia-inducible factors as molecular targets for liver diseases. J. Mol. Med. (Berl.) 94, 613–627 (2016). [PubMed: 27094811]
5. Semenza GL & Wang GL A nuclear factor induced by hypoxia via de novo protein synthesis binds to the human erythropoietin gene enhancer at a site required for transcriptional activation. Mol. Cell. Biol 12, 5447–5454 (1992). [PubMed: 1448077]
6. Ivan M et al. HIFα targeted for VHL-mediated destruction by proline hydroxylation: implications for O_2 sensing. Science 292, 464–468 (2001). [PubMed: 11292862]
7. Jaakkola P et al. Targeting of HIF-α to the von Hippel-Lindau ubiquitylation complex by O_2-regulated prolyl hydroxylation. Science 292, 468–472 (2001). [PubMed: 11292861]
8. Minamishima YA et al. A feedback loop involving the Phd3 prolyl hydroxylase tunes the mammalian hypoxic response *in vivo*. Mol. Cell. Biol 29, 5729–5741 (2009). [PubMed: 19720742]
9. Qu A et al. Hypoxia-inducible transcription factor 2α promotes steatohepatitis through augmenting lipid accumulation, inflammation, and fibrosis. Hepatology 54, 472–483 (2011). [PubMed: 21538443]
10. Ramakrishnan SK et al. HIF2α is an essential molecular brake for postprandial hepatic glucagon response independent of insulin signaling. Cell Metab. 23, 505–516 (2016). [PubMed: 26853750]
11. Taniguchi CM et al. Cross-talk between hypoxia and insulin signaling through Phd3 regulates hepatic glucose and lipid metabolism and ameliorates diabetes. Nat. Med 19, 1325–1330 (2013). [PubMed: 24037093]
12. Wei K et al. A liver Hif-2α-Irs2 pathway sensitizes hepatic insulin signaling and is modulated by Vegf inhibition. Nat. Med 19, 1331–1337 (2013). [PubMed: 24037094]
13. Gonzalez FJ, Jiang C & Patterson AD An intestinal microbiota-farnesoid X receptor axis modulates metabolic disease. Gastroenterology 151, 845–859 (2016). [PubMed: 27639801]
14. Singh V et al. Microbiota-dependent hepatic lipogenesis mediated by stearoyl CoA desaturase 1 (SCD1) promotes metabolic syndrome in TLR5-deficient mice. Cell Metab. 22, 983–996 (2015). [PubMed: 26525535]
15. Jiang C et al. Intestinal farnesoid X receptor signaling promotes nonalcoholic fatty liver disease. J. Clin. Invest 125, 386–402 (2015). [PubMed: 25500885]
16. Safran M et al. Mouse model for noninvasive imaging of HIF prolyl hydroxylase activity: assessment of an oral agent that stimulates erythropoietin production. Proc. Natl. Acad. Sci. USA 103, 105–110 (2006). [PubMed: 16373502]

17. Pagadala M, Kasumov T, McCullough AJ, Zein NN & Kirwan JP Role of ceramides in nonalcoholic fatty liver disease. Trends Endocrinol. Metab 23, 365–371 (2012). [PubMed: 22609053]
18. Kitatani K, Idkowiak-Baldys J & Hannun YA The sphingolipid salvage pathway in ceramide metabolism and signaling. Cell. Signal 20, 1010–1018 (2008). [PubMed: 18191382]
19. Jornayvaz FR & Shulman GI Diacylglycerol activation of protein kinase Cε and hepatic insulin resistance. Cell Metab. 15, 574–584 (2012). [PubMed: 22560210]
20. Xue X et al. Endothelial PAS domain protein 1 activates the inflammatory response in the intestinal epithelium to promote colitis in mice. Gastroenterology 145, 831–841 (2013). [PubMed: 23860500]
21. Wallace EM et al. A small-molecule antagonist of HIF2α is efficacious in preclinical models of renal cell carcinoma. Cancer Res. 76, 5491–5500 (2016). [PubMed: 27635045]
22. Zou Y, Albohy A, Sandbhor M & Cairo CW Inhibition of human neuraminidase 3 (NEU3) by C9-triazole derivatives of 2,3-didehydro-N-acetyl-neuraminic acid. Bioorg. Med. Chem. Lett 20, 7529–7533 (2010). [PubMed: 21036040]
23. Yoshinaga A et al. NEU3 inhibitory effect of naringin suppresses cancer cell growth by attenuation of EGFR signaling through GM3 ganglioside accumulation. Eur. J. Pharmacol 782, 21–29 (2016). [PubMed: 27105818]
24. Triner D & Shah YM Hypoxia-inducible factors: a central link between inflammation and cancer. J. Clin. Invest 126, 3689–3698 (2016). [PubMed: 27525434]
25. Kelly CJ et al. Crosstalk between microbiota-derived short-chain fatty acids and intestinal epithelial HIF augments tissue barrier function. Cell Host Microbe 17, 662–671 (2015). [PubMed: 25865369]
26. Rivera-Chávez F et al. Depletion of butyrate-producing clostridia from the gut microbiota drives an aerobic luminal expansion of salmonella. Cell Host Microbe 19, 443–454 (2016). [PubMed: 27078066]
27. Hubbard TD, Murray IA & Perdew GH Indole and tryptophan metabolism: endogenous and dietary routes to Ah receptor activation. Drug Metab. Dispos 43, 1522–1535 (2015). [PubMed: 26041783]
28. Kawano Y et al. Colonic pro-inflammatory macrophages cause insulin resistance in an intestinal Ccl2/Ccr2-dependent manner. Cell Metab. 24, 295–310 (2016). [PubMed: 27508875]
29. Rahman K et al. Loss of junctional adhesion molecule A promotes severe steatohepatitis in mice on a diet high in saturated fat, fructose, and cholesterol. Gastroenterology 151, 733–746 (2016). [PubMed: 27342212]
30. Ramakrishnan SK & Shah YM Role of intestinal HIF-2α in health and disease. Annu. Rev. Physiol 78, 301–325 (2016). [PubMed: 26667076]
31. Glover LE, Lee JS & Colgan SP Oxygen metabolism and barrier regulation in the intestinal mucosa. J. Clin. Invest 126, 3680–3688 (2016). [PubMed: 27500494]
32. Furuta GT et al. Hypoxia-inducible factor 1-dependent induction of intestinal trefoil factor protects barrier function during hypoxia. J. Exp. Med 193, 1027–1034 (2001). [PubMed: 11342587]
33. Synnestvedt K et al. Ecto-5′-nucleotidase (CD73) regulation by hypoxia-inducible factor-1 mediates permeability changes in intestinal epithelia. J. Clin. Invest 110, 993–1002 (2002). [PubMed: 12370277]
34. Robinson A et al. Mucosal protection by hypoxia-inducible factor prolyl hydroxylase inhibition. Gastroenterology 134, 145–155 (2008). [PubMed: 18166352]
35. Karhausen J et al. Epithelial hypoxia-inducible factor-1 is protective in murine experimental colitis. J. Clin. Invest 114, 1098–1106 (2004). [PubMed: 15489957]
36. Glover LE et al. Control of creatine metabolism by HIF is an endogenous mechanism of barrier regulation in colitis. Proc. Natl. Acad. Sci. USA 110, 19820–19825 (2013). [PubMed: 24248342]
37. Xie L et al. Hypoxia-inducible factor/MAZ-dependent induction of caveolin-1 regulates colon permeability through suppression of occludin, leading to hypoxia-induced inflammation. Mol. Cell. Biol 34, 3013–3023 (2014). [PubMed: 24891620]
38. Cummins EP et al. The hydroxylase inhibitor dimethyloxalylglycine is protective in a murine model of colitis. Gastroenterology 134, 156–165 (2008). [PubMed: 18166353]

39. Shah YM et al. Hypoxia-inducible factor augments experimental colitis through an MIF-dependent inflammatory signaling cascade. Gastroenterology 134, 2036–2048.e3 (2008). [PubMed: 18439915]
40. Summers SA & Goodpaster BH CrossTalk proposal: Intramyocellular ceramide accumulation does modulate insulin resistance. J. Physiol. (Lond.) 594, 3167–3170 (2016). [PubMed: 26996141]
41. Chavez JA & Summers SA A ceramide-centric view of insulin resistance. Cell Metab. 15, 585–594 (2012). [PubMed: 22560211]
42. Gorden DL et al. Biomarkers of NAFLD progression: a lipidomics approach to an epidemic. J. Lipid Res 56, 722–736 (2015). [PubMed: 25598080]
43. Haus JM et al. Plasma ceramides are elevated in obese subjects with type 2 diabetes and correlate with the severity of insulin resistance. Diabetes 58, 337–343 (2009). [PubMed: 19008343]
44. Chaurasia B & Summers SA Ceramides—lipotoxic inducers of metabolic disorders. Trends Endocrinol. Metab 26, 538–550 (2015). [PubMed: 26412155]
45. Xia JY et al. Targeted induction of ceramide degradation leads to improved systemic metabolism and reduced hepatic steatosis. Cell Metab. 22, 266–278 (2015). [PubMed: 26190650]
46. Turpin SM et al. Obesity-induced CerS6-dependent C16:0 ceramide production promotes weight gain and glucose intolerance. Cell Metab. 20, 678–686 (2014). [PubMed: 25295788]
47. Raichur S et al. CerS2 haploinsufficiency inhibits β-oxidation and confers susceptibility to diet-induced steatohepatitis and insulin resistance. Cell Metab. 20, 687–695 (2014). [PubMed: 25295789]
48. Holland WL et al. Inhibition of ceramide synthesis ameliorates glucocorticoid-, saturated-fat-, and obesity-induced insulin resistance. Cell Metab. 5, 167–179 (2007). [PubMed: 17339025]
49. Chaurasia B et al. Adipocyte ceramides regulate subcutaneous adipose browning, inflammation, and metabolism. Cell Metab. 24, 820–834 (2016). [PubMed: 27818258]
50. Jiang C et al. Intestine-selective farnesoid X receptor inhibition improves obesity-related metabolic dysfunction. Nat. Commun 6, 10166(2015). [PubMed: 26670557]
51. Perry RJ, Samuel VT, Petersen KF & Shulman GI The role of hepatic lipids in hepatic insulin resistance and type 2 diabetes. Nature 510, 84–91 (2014). [PubMed: 24899308]
52. Samuel VT & Shulman GI Mechanisms for insulin resistance: common threads and missing links. Cell 148, 852–871 (2012). [PubMed: 22385956]
53. Giussani P, Tringali C, Riboni L, Viani P & Venerando B Sphingolipids: key regulators of apoptosis and pivotal players in cancer drug resistance. Int. J. Mol. Sci 15, 4356–4392 (2014). [PubMed: 24625663]
54. Yoshizumi S et al. Increased hepatic expression of ganglioside-specific sialidase, NEU3, improves insulin sensitivity and glucose tolerance in mice. Metabolism 56, 420–429 (2007). [PubMed: 17292733]
55. Scaringi R et al. NEU3 sialidase is activated under hypoxia and protects skeletal muscle cells from apoptosis through the activation of the epidermal growth factor receptor signaling pathway and the hypoxia-inducible factor (HIF)-1α. J. Biol. Chem 288, 3153–3162 (2013). [PubMed: 23209287]
56. Cho H et al. On-target efficacy of a HIF2α antagonist in preclinical kidney cancer models. Nature 539, 107–111 (2016). [PubMed: 27595393]
57. Chen W et al. Targeting renal cell carcinoma with a HIF-2 antagonist. Nature 539, 112–117 (2016). [PubMed: 27595394]
58. Haase VH, Glickman JN, Socolovsky M & Jaenisch R Vascular tumors in livers with targeted inactivation of the von Hippel-Lindau tumor suppressor. Proc. Natl. Acad. Sci. USA 98, 1583–1588 (2001). [PubMed: 11171994]
59. Anderson ER et al. The hypoxia-inducible factor-C/EBPα axis controls ethanol-mediated hepcidin repression. Mol. Cell. Biol 32, 4068–4077 (2012). [PubMed: 22869521]
60. Hu CJ, Sataur A, Wang L, Chen H & Simon MC The N-terminal transactivation domain confers target gene specificity of hypoxia-inducible factors HIF-1α and HIF-2α. Mol. Biol. Cell 18, 4528–4542 (2007). [PubMed: 17804822]

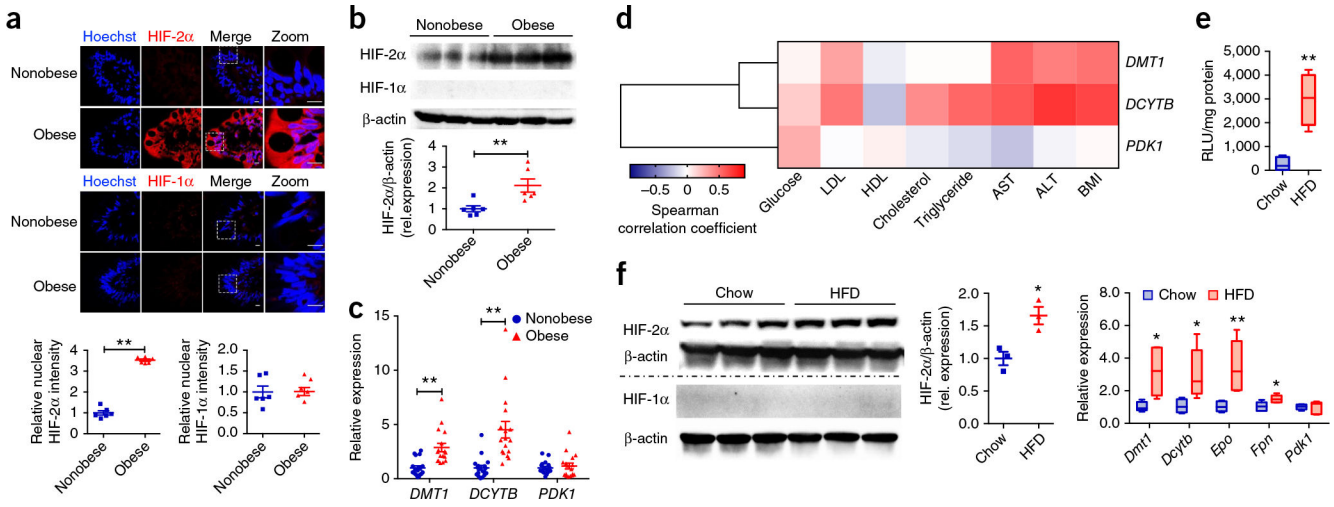

Figure 1.

Increased HIF-2α signaling in human ileum biopsies is correlated with obesity. (**a**) Representative immunohistochemical staining for the expression of HIF-2α and HIF-1α in human ileum biopsies from cohort 1 ($n = 6$ subjects/group, 3 images/subject). (**b**) Representative western blot analysis of HIF-2α and HIF-1α protein expression in three individual ileum biopsies from cohort 1. $n = 6$/group for blot quantification. (**c**) mRNA expression levels of HIF-2α target gene *DMT1*, *DCYTB*, and HIF-1α target gene *PDK1* in human ileum biopsies from individuals without obesity ($n = 18$) and with obesity ($n = 17$) (cohort 2). $^{**}P < 0.01$, relative nonobese individuals, by two-tailed Student's *t*-test. (**d**) Heat map of the correlative analysis of *DMT1*, *DCYTB*, and *PDK1* mRNAs in human ileum biopsies (cohort 2) with BMI and clinical biochemistry parameters ($n = 35$). Correlations were assessed by nonparametric Spearman's test. (**e**) The relative luciferase activities in small intestine (ileum) from ODD-luciferase transgenic mice fed a chow diet or HFD ($n = 4$/group). (**f**) Western blot analysis of HIF-2α and HIF-1α protein expression ($n = 3$/group) and mRNA expression analysis ($n = 5$/group) of their target genes in small intestine from chow-diet or HFD-fed mice (8 weeks). Data are presented as mean ± s.e.m. For box plots, the midline represents the median; box represents the interquartile range (IQR) between the first and third quartiles, and whiskers represent the lowest or highest values within 1.5 times interquartile range (IQR) from the first or third quartiles. $^{*}P < 0.05$, $^{**}P < 0.01$ relative to a chow diet, by two-tailed Student's *t*-test.

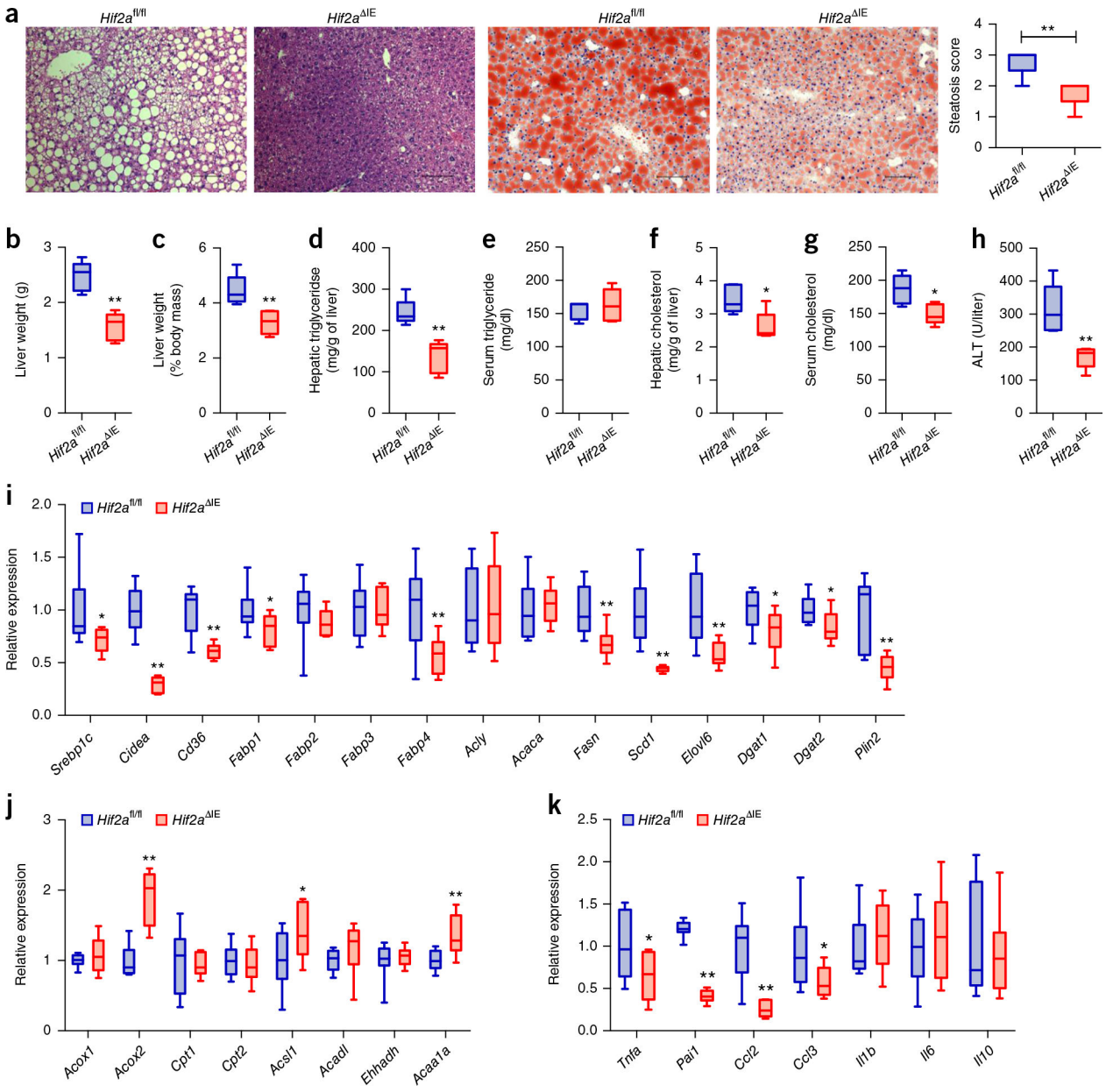

Figure 2.

Intestine-specific HIF-2α disruption ameliorates the development of hepatic steatosis. (**a**) Representative H&E staining (left two panels) and Oil Red O staining (right two panels) of liver sections (n = 5 mice/group, 3 images/mouse). Scale bars, 100 μm. (**b**) Liver weights. (**c**) Liver weight–to–body weight ratios. (**d,e**) Liver (**d**) and serum (**e**) triglyceride content. (**f,g**) Liver (**f**) and serum (**g**) cholesterol content. (**h**) Serum ALT levels. (**i**) Hepatic expression of mRNAs encoded by hepatic fatty acid transport and lipogenesis-related genes. (**j**) Hepatic expression of mRNAs encoded by hepatic fatty acid β-oxidation-related genes. (**k**) Hepatic expression of mRNAs encoded by inflammatory cytokine and chemokine genes. HFD-fed *Hif2a*$^{fl/fl}$ and *Hif2a*$^{\Delta IE}$ mice. n = 5/group. For box plots, the midline represents the median; box represents the IQR between the first and third quartiles, and whiskers represent

the lowest or highest values within 1.5 times IQR from the first or third quartiles. $*P < 0.05$, $**P < 0.01$ relative to *Hif2a*$^{fl/fl}$ mice, by two-tailed Student's *t*-test.

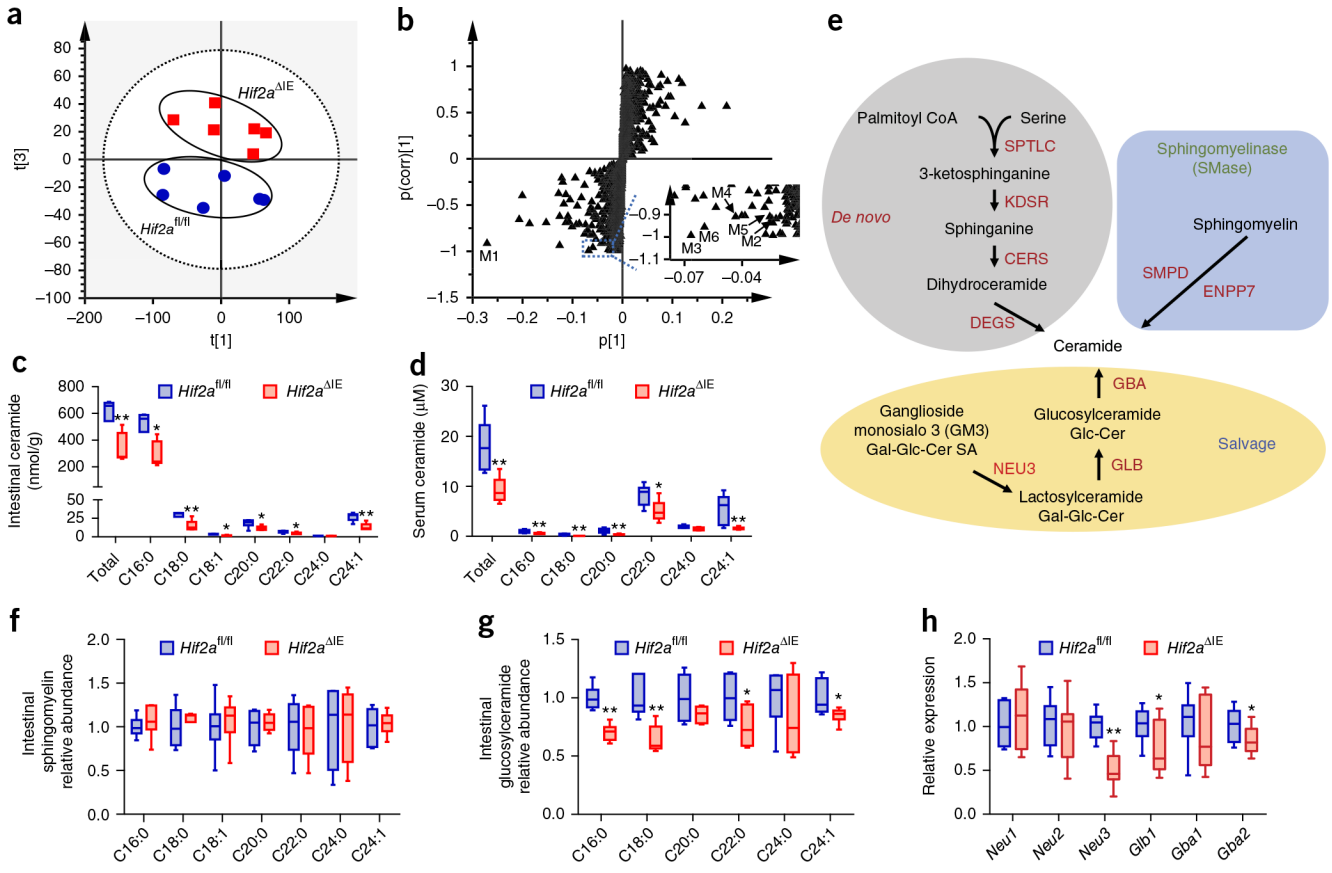

Figure 3.

Intestinal HIF-2α deficiency reduces ceramide synthesis in the small intestine. (**a**) Score scatter plot of a PCA model of the intestinal metabolites between *Hif2a*$^{fl/fl}$ (circle) and *Hif2a*$^{\Delta IE}$ (square) mice. Each point represents an individual mouse sample. (**b**) S-plot of an orthogonal partial least-squares discriminant analysis (OPLS-DA) model of the intestinal metabolites. Each point represents a metabolite ion. Insert shows a scaled region with metabolites M2–M6. (**c,d**) Quantitation of ceramide concentrations in the small intestine (**c**) and serum (**d**). (**e**) Scheme for ceramide-synthesis pathways. (**f,g**) The relative levels of sphingomyelin (**f**) and glucosylceramide (**g**) in the small intestine. (**h**) Intestinal expression of intestinal mRNAs encoding ceramide salvage-related enzymes. *Hif2a*$^{fl/fl}$ and *Hif2a*$^{\Delta IE}$ mice fed a HFD for 12 weeks. $n = 6$/group. Data are presented as mean ± s.e.m. For box plots, the midline represents the median; box represents the IQR between the first and third quartiles, and whiskers represent the lowest or highest values within 1.5 times IQR from the first or third quartiles. *$P < 0.05$, **$P < 0.01$ relative to *Hif2a*$^{fl/fl}$ mice, by two-tailed Student's *t*-test.

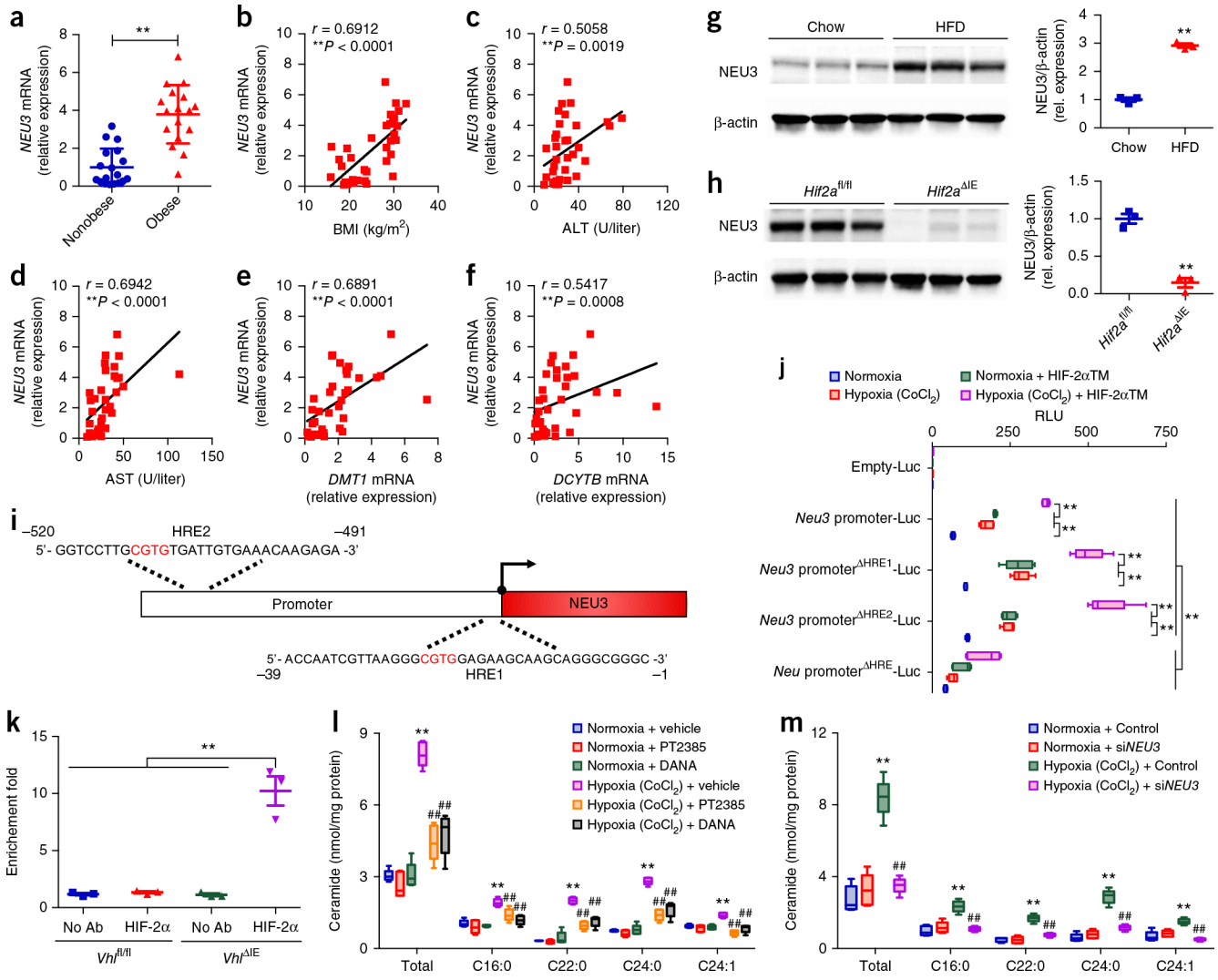

Figure 4.

The ceramide-synthesis-related gene *Neu3* is a novel HIF-2α target gene in the small intestine. (**a**) Expression of *NEU3* mRNA in human ileum biopsies from nonobese individuals ($n = 18$) and individuals with obesity ($n = 17$) (cohort 2). $^{**}P < 0.01$, versus healthy subjects, by two-tailed Student's *t*-test. (**b–f**) Correlative analysis of ileum *NEU3* mRNA levels with BMI (**b**), ALT (**c**), AST (**d**), *DMT1* mRNA (**e**), and *DCYTB* mRNA (**f**). $n = 35$. Correlations were assessed by nonparametric Spearman's test. (**g**) Western blot analysis of NEU3 protein expression in small intestine of chow-diet or HFD-fed mice (8 weeks, $n = 3$/group). (**h**) Western blot analysis of NEU3 protein expression in the small intestine of HFD fed-*Hif2a*$^{fl/fl}$ and *Hif2a*$^{\Delta IE}$ mice (12 weeks, $n = 3$/group). Data are presented as means ± s.e.m. $^{**}P < 0.01$ relative to *Hif2a*$^{fl/fl}$ mice, by two-tailed Student's *t*-test. (**i**) Schematic diagram of the mouse *Neu3* promoter illustrating the HREs in the regulatory region; the upstream regions are numbered in relation to the transcription initiation site, which is designated +1. (**j**) Luciferase-reporter gene assay of *Neu3* promoter activity ($n = 5$/group). $^{**}P < 0.01$, by two-tailed Student's *t*-test. (**k**) *In vivo* ChIP assays on small intestinal extracts from *Vhl*$^{fl/fl}$ and *Vhl*$^{\Delta IE}$ mice ($n = 3$/group). $^{**}P < 0.01$, by two-

tailed Student's *t*-test. (**l**) Ceramide levels in HCT116 cells treated with vehicle, PT2385, or DANA and exposed to either vehicle or $CoCl_2$ (n = 5/group). $^{**}P < 0.01$ relative to normoxia + vehicle, $^{\#\#}P < 0.01$ relative to hypoxia ($CoCl_2$) + vehicle, by one-way ANOVA with Tukey's correction. (**m**) Ceramide levels in HCT116 cells transfected with control or si*NEU3* and exposed to either vehicle and $CoCl_2$ (n = 5/group). $^{**}P < 0.01$ versus normoxia + control, $^{\#\#}P < 0.01$ versus hypoxia ($CoCl_2$) + control, by one-way ANOVA with Tukey's correction. Data are presented as mean ± s.e.m. For box plots, the midline represents the median; box represents the IQR between the first and third quartiles, and whiskers represent the lowest or highest values within 1.5 times IQR from the first or third quartiles.

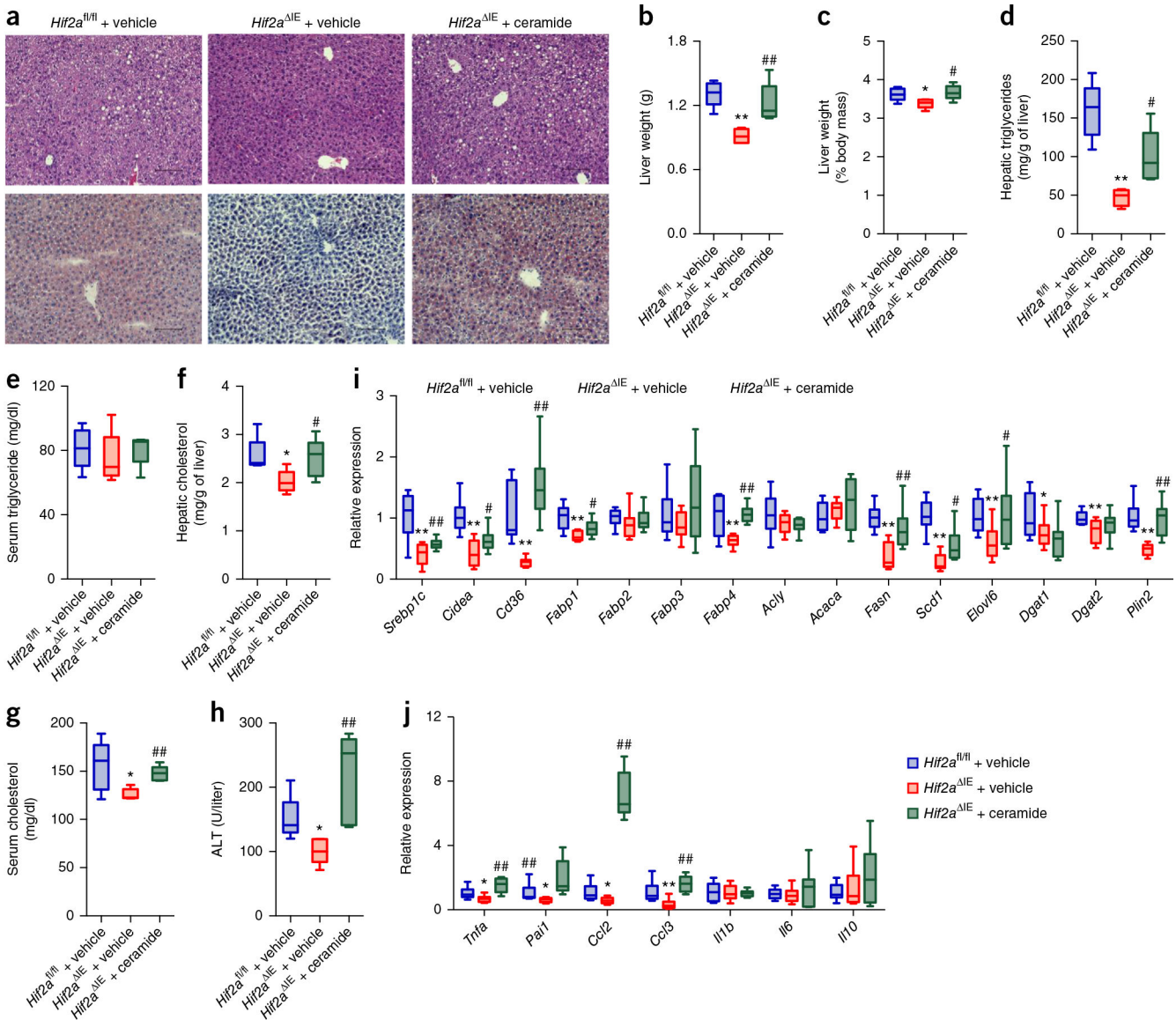

Figure 5.

Administration of ceramide reverses the protective effects of intestinal HIF-2α inhibition on the development of HFD-induced hepatic steatosis. (**a**) Representative H&E staining (upper) and Oil Red O staining (lower) of liver sections (n = 5 mice/group, 3 images/mouse). Scale bars, 100 μm. (**b**) Liver weights. (**c**) Liver weight–to–body weight ratios. (**d,e**) Liver (**d**) and serum (**e**) triglyceride content. (**f,g**) Liver (**f**) and serum (**g**) cholesterol content. (**h**) Serum ALT levels. (**i**) Hepatic expression of mRNAs encoded by hepatic fatty acid transport and lipogenesis-related genes. (**j**) Hepatic expression of mRNAs encoded by inflammatory cytokine and chemokine genes. Ceramide-treated HFD-fed *Hif2a*$^{fl/fl}$ and *Hif2a*$^{\Delta IE}$ mice. n = 5/group. For box plots, the midline represents the median; box represents the IQR between the first and third quartiles, and whiskers represent the lowest or highest values within 1.5 times IQR from the first or third quartiles. *P < 0.05, **P < 0.01 relative to vehicle-treated

Hif2a$^{fl/fl}$ mice, #$P < 0.05$, ##$P < 0.01$ relative to vehicle-treated *Hif2a*$^{\Delta IE}$ mice, by one-way ANOVA with Tukey's correction.

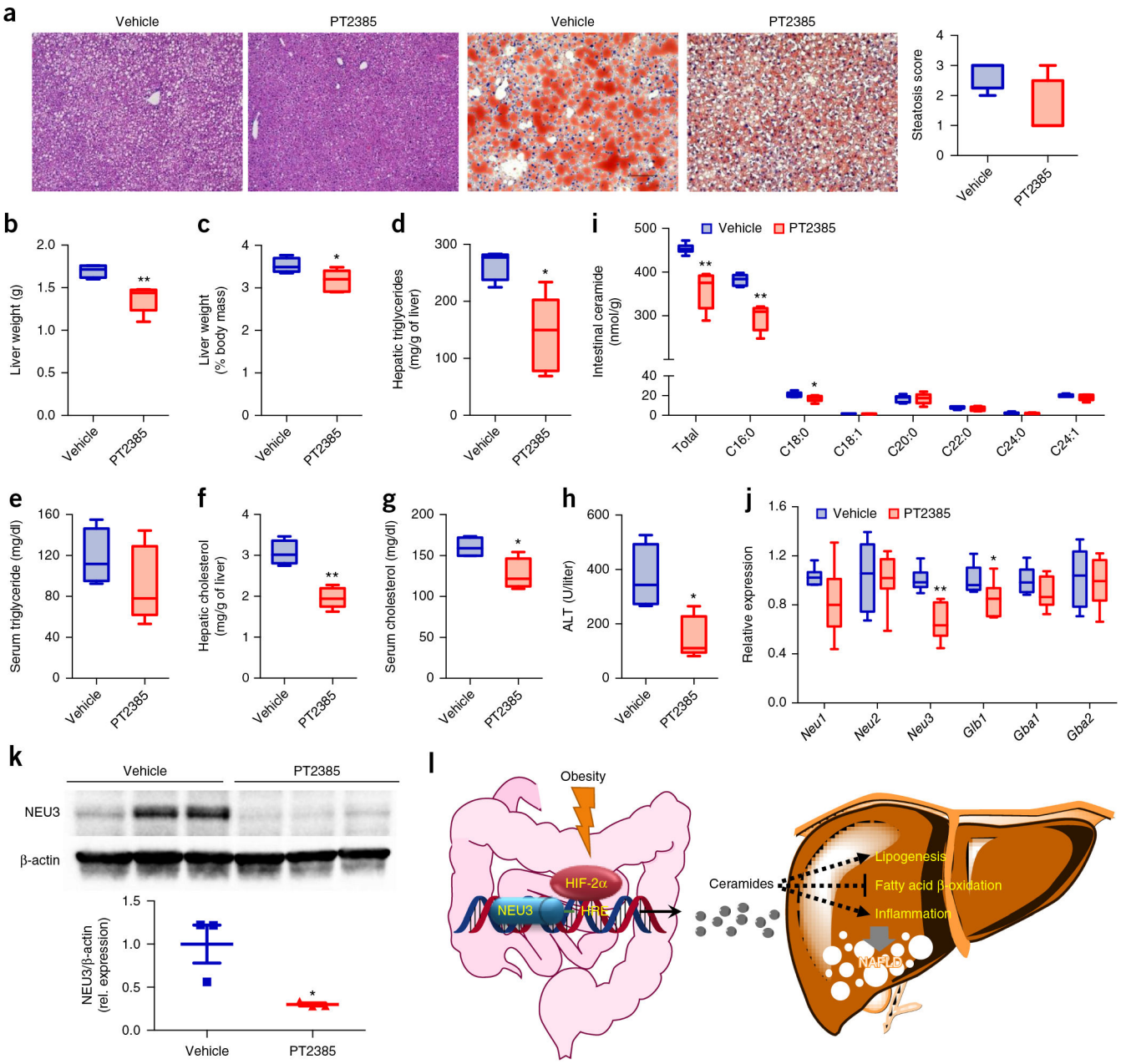

Figure 6.

PT2385 reverses HFD-induced hepatic steatosis. (**a**) Representative H&E staining (left two panels) and Oil Red O staining (right two panels) of liver sections ($n = 4$ mice for vehicle group, $n = 5$ mice for PT2385 group, 3 images/mouse). Lipids stain positive (red color) with Oil Red O. Scale bars, 100 μm. $P = 0.06$ for steatosis score. (**b**) Liver weights. (**c**) Liver weight–to–body weight ratios. (**d,e**) Liver (**d**) and serum (**e**) triglyceride content. (**f,g**) Liver (**f**) and serum (**g**) cholesterol content. (**h**) Serum ALT levels. (**i**) Quantitation of ceramide concentrations in the small intestine. (**j**) Intestinal expression of mRNAs encoding ceramide salvage-related enzymes. PT2385-treated HFD-fed mice with obesity. $n = 4$ for vehicle group, $n = 5$ for PT2385 group. For box plots, the midline represents the median; box

represents the IQR between the first and third quartiles, and whiskers represent the lowest or highest values within 1.5 times IQR from the first or third quartiles. (**k**) Western blot analysis of NEU3 protein expression in the small intestine (n = 3/group). (**l**) A schematic diagram summarizing the findings that obesity promotes a HIF-2α–NEU3–ceramide pathway that contributes to NAFLD progression. Data are presented as mean ± s.e.m. *P < 0.05, **P < 0.01 relative to vehicle treatment, by two-tailed Student's t-test.